Device design and materials optimization of conformal coating for islets of Langerhans

Alice A. Tomei[a,1], Vita Manzoli[a,b], Christopher A. Fraker[a], Jaime Giraldo[a,c], Diana Velluto[d], Mejdi Najjar[a], Antonello Pileggi[a], R. Damaris Molano[a], Camillo Ricordi[a], Cherie L. Stabler[a,c], and Jeffrey A. Hubbell[a,d]

[a]Diabetes Research Institute, University of Miami Miller School of Medicine, Miami, FL 33136; [b]Department of Electronics, Information and Bioengineering, Politecnico di Milano, 20133 Milan, Italy; [c]Department of Biomedical Engineering, College of Engineering, University of Miami, Coral Gables, FL 33146 and [d]Institute of Bioengineering, École Polytechnique Fédérale de Lausanne, 1015 Lausanne, Switzerland

Edited by Mark E. Davis, California Institute of Technology, Pasadena, CA, and approved June 10, 2014 (received for review February 5, 2014)

Encapsulation of islets of Langerhans may represent a way to transplant islets in the absence of immunosuppression. Traditional methods for encapsulation lead to diffusional limitations imposed by the size of the capsules (600–1,000 μm in diameter), which results in core hypoxia and delayed insulin secretion in response to glucose. Moreover, the large volume of encapsulated cells does not allow implantation in sites that might be more favorable to islet cell engraftment. To address these issues, we have developed an encapsulation method that allows conformal coating of islets through microfluidics and minimizes capsule size and graft volume. In this method, capsule thickness, rather than capsule diameter, is constant and tightly defined by the microdevice geometry and the rheological properties of the immiscible fluids used for encapsulation within the microfluidic system. We have optimized the method both computationally and experimentally, and found that conformal coating allows for complete encapsulation of islets with a thin (a few tens of micrometers) continuous layer of hydrogel. Both in vitro and in vivo in syngeneic murine models of islet transplantation, the function of conformally coated islets was not compromised by encapsulation and was comparable to that of unencapsulated islets. We have further demonstrated that the structural support conferred by the coating materials protected islets from the loss of function experienced by uncoated islets during ex vivo culture.

cell encapsulation | polyethylene glycol | alginate | cell transplantation

Islet cell transplantation shows great promise for the treatment of type 1 diabetes; however, it requires life-long systemic immunosuppression, which is (*i*) not completely effective, (*ii*) detrimental to islet cell function, and (*iii*) the primary cause of adverse events (1). Due to the suboptimal efficacy and safety associated with the procedure, islet transplantation is currently limited to cases of extreme necessity. Immunoisolation via cell encapsulation may allow transplantation without SI and increase the safety and clinical impact of the procedure (2–5). Although encapsulation has been studied for the past 50 y (6), its clinical success, thus far, has been limited (2, 4, 7–12). Among the possible reasons for the failure of immunoisolation technologies are the large size (between 600 μm and 3 mm), which results in diffusional gradients and large implant volumes, and the instability of conventional encapsulation materials. Molecules that are critical for islet survival and function, including oxygen, nutrients, and insulin, are exchanged through diffusion across the polymeric capsule (13). Such passive transport is limited to a distance of ∼150 μm, which is significantly (∼10–50%) smaller than the half-length/radial distance of most devices (14, 15). Diffusion limitations may result in blunted secretion of trophic factors in response to host stimulation (e.g., insulin in response to elevations in glucose) and in core necrosis. Moreover, transplant sites able to accommodate such large volumes are restricted to the intraperitoneal. space, which is poorly vascularized and therefore less favorable to cell engraftment (16–18). Finally, materials used for conventional microencapsulation are based on alginate (ALG) hydrogels whose stability in vivo, including permselectivity to cytokines, antibodies, and cells, has been long argued (2, 4, 19).

To address these issues, investigators have focused on developing methods and technologies to minimize coating thickness and increase capsule stability (20, 21). Among these technologies are PEGylation (22), layer-by-layer (23–27), and conformal coating (28–32), which are based on chemically reacting hydrogels directly to the cell surface (21, 33, 34), as well as the development of ALG derivatives with enhanced performance (35). Although successful in vitro, most technologies have not achieved success as immune barriers in preclinical and clinical models, still requiring systemic immunosuppression (36).

Here, we sought to develop a unique approach for the conformal coating (i.e., conforms to the shape and size of the encapsulated material, resulting in coatings uniform in thickness) of islets with PEG hydrogels. Because islets are of highly variable size, it would be beneficial if the coatings were conformal, with a similar thickness on each islet rather than a similar capsule diameter independent of islet size (Fig. 1*A*). The concept explored was to use a flow-focusing method to coat individual islets conformally within a hydrogel precursor, and then to cross-

Significance

Cell encapsulation with biocompatible and permeable hydrogels may allow transplantation without immunosuppression. As an alternative to standard microencapsulation approaches that create single-sized capsules around cell clusters of different sizes, we have designed and optimized a novel approach for conformal coating of islets of Langerhans, resulting in thin, complete, and uniform coatings of similar thickness on differently sized islets. Coated islets exhibited no delay in glucose-stimulated insulin release or loss of function during culture, which is often observed with naked islets. The conformal coating reduces transplant volume relative to traditional encapsulation approaches. When transplanted in syngeneic diabetic mice, conformally coated islets restored and maintained euglycemia for more than 100 d with no foreign body reaction and normal revascularization.

Author contributions: A.A.T., A.P., C.R., C.L.S., and J.A.H. designed research; A.A.T., V.M., C.A.F., J.G., D.V., M.N., and R.D.M. performed research; A.A.T., V.M., C.A.F., and C.L.S. analyzed data; A.A.T. and J.A.H. wrote the paper; and A.A.T. and J.A.H. directed the project.

Conflict of interest statement: A.A.T. and J.A.H. are coinventors of intellectual property used in the study and may gain royalties from future commercialization of the technology licensed to Converge Biotech, Inc. A.P., C.R. and C.L.S. are members of the scientific advisory board and stock option holders in Converge Biotech, Inc., licensee of some of the intellectual property used in this study. R.D.M. is a stock option holder in Converge Biotech, Inc.

This article is a PNAS Direct Submission.

Freely available online through the PNAS open access option.

[1]To whom correspondence should be addressed. Email: atomei@med.miami.edu.

This article contains supporting information online at www.pnas.org/lookup/suppl/doi:10.1073/pnas.1402216111/-/DCSupplemental.

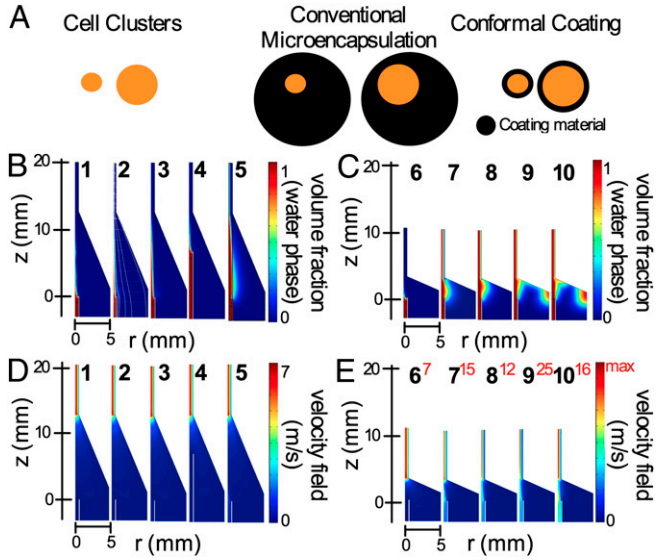

Fig. 1. Computational model of the conformal coating procedure for optimization of the fluid dynamic conditions and the design of the encapsulation device. (*A*) Schematic of conformal coating encapsulation of islets compared with conventional microencapsulation. Comsol plots of the water-phase volume fraction for models 1–5 (*B*; "less focusing") and 6–10 (*C*; "more focusing") and the velocity field for models 1–5 (*D*) and 6–10 (*E*) as a function of the *z* axis and r radius are shown.

link the precursor into an elastic hydrogel. The method allows for the "shrink-wrapping" of cell clusters with minimal amounts of coating materials by means of microfluidic templating, followed by chemical cross-linking of the liquid hydrogel precursor surrounding the islet to form a stable gel. Computational models were developed to optimize microfluidic chamber design and fluid dynamic variables. The modeling results were then confirmed experimentally with islet-simulating beads and pancreatic islets. In vitro glucose-stimulated insulin release (GSIR) and perifusion assays and syngeneic islet transplants under the kidney capsule of diabetic mice were used as functional readouts.

Results

Flow Focusing for Conformal Coating of Cell Clusters. High-throughput encapsulation of individual cell clusters into nanoliter droplets of PEG gel (conformal coating) was accomplished by exploiting the Raleigh–Plateau instability generated when a water phase is flowing in a coaxial jet within an immiscible oil phase. To generate a stable jet of water in oil, a dripping-to-jetting transition was induced in the water phase by focusing the external oil phase through external physical constraints, with a conical flow of reducing diameter in this study. The Rayleigh–Plateau instability then produces a disruption of the water-phase jet into droplets that have a characteristic size (nanoliters) proportional to the water jet size and dependent on (*i*) the water- and oil-phase flow rate ratio, (*ii*) the water- and oil-phase viscosity ratio, and (*iii*) the interfacial tension between the two phases (37). When particulates, islets of Langerhans in this study, are added to the inner water phase, their entrance in the focusing region induces an upstream rupture of the water jet, resulting in individual islet coating. Irrespective of islet size, the coating thickness is proportional to the size of the nanoliter droplets that are generated in the absence of particulates. Additionally, because the islet diameter is typically bigger than the water jet diameter, islets are kept separate from each other by the elongational component of the flow in the focusing region. Even in cases of elevated cell density, this property individually aligns islets in the center of the jet and maintains their separation, ultimately allowing for the encapsulation of single islets within single droplets, thus achieving conformal coating (Fig. 1*A*).

A microfluidic chamber and technique were developed to achieve the desired dripping-to-jetting transition of the islet/hydrogel precursor solution [water phase (w)] within the immiscible oil phase (o) and to disrupt the resulting water-phase jet into the desired nanoliter droplets ideal for conformal coating of individual islets. Using previously published work (38–40) and fluid dynamic finite element modeling (Comsol multiphysics), combinations of geometric and hydrodynamic parameter estimates of the oil and water phases were generated and screened to determine optimal settings for water-phase jet generation within the oil phase. Two model flow chamber designs with a total of 10 different combinations of geometric and hydrodynamic parameters, summarized in Table 1, were simulated. Device geometries tested, together with the chosen computational meshes, are shown in Fig. S1*A*. Three variations of the focusing/injection distance were tested: reduced focusing/standard injection distance of the water phase (a), increased focusing/standard injection distance (b), and reduced focusing and closer injection distance (c).

Based on the model developed by Suryo and Basaran (38), jetting of the water phase was predicted to occur for every combination of parameters tested and is shown in Table 1. This prediction is partly confirmed by the results from our simulations, which show that, depending on the different combinations of geometric and hydrodynamic parameters, jets of water with different characteristics can be generated (Fig. 1 *B* and *C*; the volume fraction of the water phase is plotted). In particular, when using the less focused jet geometry (Fig. 1*B*) with a medium viscosity (η) oil phase, jetting of the water phase was achieved when $v_w = v_o$ (model 2), whereas when $v_w = v_o/5$ (model 1),

Table 1. List of combinations of geometric and hydrodynamic parameters simulated

No.	γ, N/m	η_2, Pa * s	η_1, Pa * s	v_2, m/s	v_1, m/s	Q_R	1/Ca	mQ_R	WIP	FG	T_r, dyn/cm^2	T_z, dyn/cm^2
1	0.005	0.34	0.01	5×10^{-2}	1×10^{-2}	347.22	49.50	11,805.56	Standard	Less	$2 * 10^6$	−60	60
2	0.005	0.34	0.01	5×10^{-2}	5×10^{-2}	69.44	9.90	2,361.11	Standard	Less	$2 * 10^6$	−10	20
3	0.005	1.301	0.01	5×10^{-2}	5×10^{-2}	69.44	9.90	9,034.72	Standard	Less	$7.5 * 10^6$	−10	50
4	0.005	1.301	0.01	5×10^{-2}	5×10^{-2}	69.44	9.90	9,034.72	Closer	Less	$7.5 * 10^6$	−10	30
5	0.005	1.301	0.01	5×10^{-2}	50×10^{-2}	6.94	0.99	903.47	Standard	Less	$8 * 10^6$	150	150
6	0.005	0.34	0.01	5×10^{-2}	1×10^{-2}	347.22	49.50	11,805.56	Standard	More	$2 * 10^6$	−45	7
7	0.005	1.301	0.01	1×10^{-2}	125×10^{-2}	0.56	0.40	72.28	Standard	More	$6 * 10^6$	10	10
8	0.005	1.301	0.01	1×10^{-2}	350×10^{-2}	0.20	0.14	25.81	Standard	More	$5 * 10^6$	30	30
9	0.005	1.301	0.01	1×10^{-2}	700×10^{-2}	0.10	0.07	12.91	Standard	More	$3.5 * 10^6$	−25	25

$1/Ca = \mu_1 Q_1/\gamma\pi R_1^2$, inverse of capillary number; η_1, water viscosity; η_2, oil viscosity; FG, focusing geometry; γ, interfacial tension; m, viscosity ratio; No., number of simulated model; Q_1, water flow rate; Q_2, oil flow rate; Q_R, Q_2/Q_1; T_r, maximum radial stress; T_z, maximum z stress; v_1, maximum water velocity; v_2, maximum oil velocity; WIP, water injection point.

the water phase shifted to dripping. When a higher viscosity oil phase was used, and $v_w = v_o$, a jet with a higher diameter was achieved (model 3). This result occurs independent of the injection point of the water phase [i.e., with the standard injection point (models 1, 2, 3, and 5) or with the injection point closer to the downstream channel (model 4)]. If, however, $v_w = 10v_o$ (model 5), the size of the water jet and the stream area from the injection point were increased, resulting in a larger and less focused jet. When using the more focused geometry (Fig. 1*C*) and a medium viscosity oil phase, jetting of the water phase was achieved even when $v_w = v_o/5$ (model 6). Increasing v_w/v_o proportionally increased the diameter of the water-phase jet (models 7–9). The stream area from the injection point was also increased and resulted in water-phase entrapment within the external part of the chamber (model 9). This entrapment could not be avoided even if the viscosity of the water phase was increased 10-fold, representative of the presence of particulates in the water phase (model 10).

In the less focused geometry, the velocity fields were not as affected by parametric variations (Fig. 1*D*, models 1–5) as they were when the more focused chamber was used, with significantly increased v_w/v_o ratios (Fig. 1*E*, models 6–9) and viscosity of the water phase (model 10).

For each simulation, the radial components (f_r) and axial components (f_z) of the total force per area on the central axis ($r = 0$) could be predicted (Fig. S1 *B* and *C*). For the less focused geometry (Fig. 1*B*), f_r decreased linearly with cylindrical axis (z), with water jet development occurring at higher values (at $z = 0$) for high oil-phase viscosity (Fig. 1*B*, models 3–5) than for middle oil-phase viscosity (models 1 and 2). At the same time, in middle oil- phase viscosity (model 1 and partially in model 2), f_z oscillated between positive and negative values, suggesting a dripping profile for the water phase. In the higher oil-phase viscosity (models 3–5), f_z became more stable with consistently positive values, achieving maximum values with higher v_w/v_o (model 5). In the more focused geometry (Fig. 1*C*), f_r decreased linearly with z, with water jet development starting at both higher values of v_w/v_o at $z = 0$ (Fig. 1*C*, models 7–9) and higher water-phase viscosity (model 10). By varying both v_w/v_o and the viscosity of the oil and water phases (models 6–10), f_z was greatly affected. Minimal absolute values were obtained in model 6.

From this computational analysis, we concluded that the desired water-phase jetting from a coaxially flowing oil phase was achieved with geometries of different stream focusing. The position of the water-phase injection tip did not affect the fluidic outcome. Using oil phases of higher viscosity facilitated jet formation, particularly with the less focused geometry. This was the case even with decreased water-phase velocities and resultant minimal pressure drop values.

Validation of Modeling and Flow Chamber: Conformal Coating of Model Beads. Following fabrication of the coating device (Fig. 2*A* and *SI Materials and Methods*), the next phase focused on the generation of the hydrogel conformal coatings. To achieve complete encapsulation of islets flowing within the water phase (which includes the hydrogel precursor and the cross-linker), break-up of the islet-containing water phase must occur before the initiation of gel polymerization through cross-linking. An eight-arm 10-kDa PEG functionalized with vinyl sulfone (VS) was selected as the gel precursor. The VS-reactive groups can be cross-linked through reaction with DTT. Exploiting the pH sensitivity of this reaction, the PEG-VS was mixed with DTT at a slightly acidic pH of 6 and triethanolamine (TEOA) was placed in the oil phase of the collection vessel downstream encapsulation to drive polymerization. Polypropylene glycol (PPG) was used as the oil phase. An oil-soluble surfactant [10% (vol/vol) Span80] was added to the oil phase to reduce surface tension to the desired value.

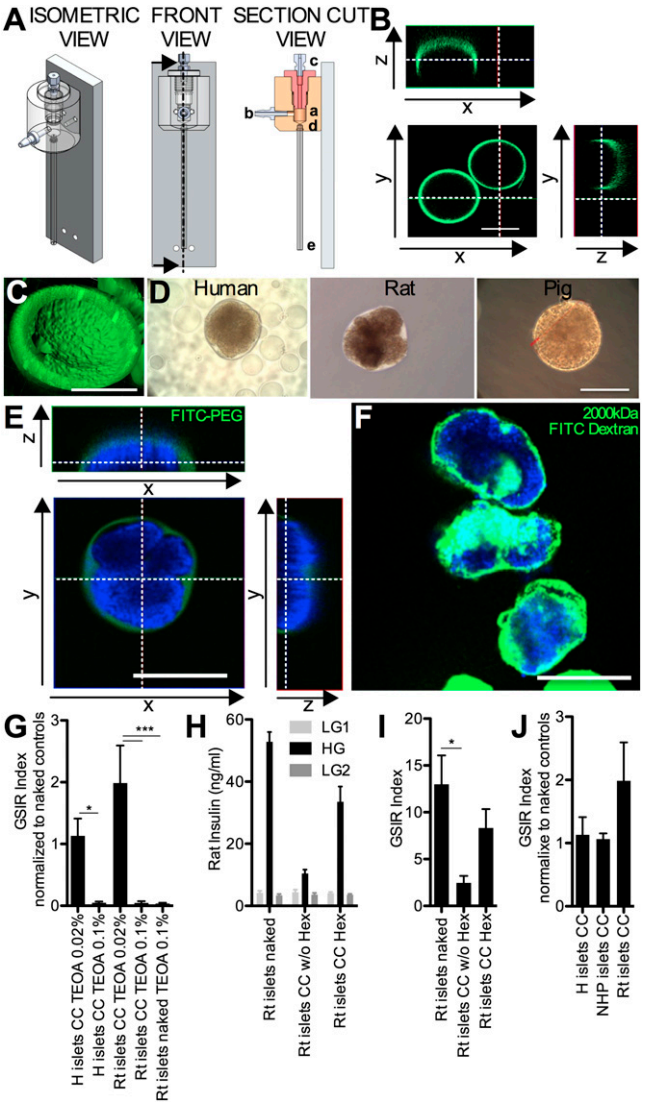

Fig. 2. Design of the flow chamber and optimization of conformal coating encapsulation of model beads and pancreatic islets with PEG-VS cross-linked with DTT. (*A*) computer-aided design (CAD) drawings of the encapsulation chamber in isometric, front, and section cut views. Orthogonal projections (*B*) and a 3D surface plot (*C*) of islet model beads conformally coated with FITC-labeled PEG. (Scale bar, 200 μm.) (*D*) Phase-contrast images of conformally coated human, rat, and pig islets. (Scale bar, 100 μm.) Orthogonal projections (*E*) and maximum projection on the *z* axis (*F*) of rat islets conformally coated with FITC-labeled PEG (*E*) or with a solution of PEG containing 1 mg/mL 2,000-kDa FITC dextran (*F*). (Scale bars, 200 μm.) (*G*) Effect of different percentages of TEOA in the PPG oil outer bath on GSIR function of conformally coated (CC) human and rat islets. (*H* and *I*) Effect of hexane (Hex) purification of CC rat islets on GSIR function. (*J*) GSIR index (normalized to naked controls) of human (H), nonhuman primate (NHP), and rat (Rt) islets CC with 0.02% TEOA and purified with hexane. Low glucose (LG) = 2.2 mM and high glucose (HG) = 16.7 mM. Shown are mean ± SD with $n = 3$ for each value. $^*P < 0.05$; $^{***}P < 0.01$.

Initial encapsulation studies were carried out with idealized spherical beads as models of cell clusters, using sizes typical of islets of Langerhans (i.e., 50–400 μm). In preliminary studies with 10% (wt/vol) PEG-VS, it was determined that conformal coating was optimal when the more focused chamber geometry was implemented with a vertical configuration (Fig. 2*A*) and the following flow rates (Q) were used: $Q_w = 10$ μL/min and $Q_o = 3.5$ mL/min (which gives a velocity ratio, $V_o/V_w = 3.5$, with cross

sectional area of the oil phase (A_o) = 100 × A_w and Q = V × A). TEOA at 0.2% was included in the collection vessel. Resulting conformally coated beads were purified from the oil phase by repeated exposure of the collected exudate to hexane, followed by hexane/HBSS washes with centrifugation, as described in *Materials and Methods*.

Coating completeness was confirmed in selected procedures by fluorescent labeling (using FITC-labeled PEG-VS) of the coatings (Fig. 2 *B* and *C*). As illustrated, the constructed encapsulation system, using parameters designed via modeling, generated the right combination of hydrodynamic conditions to achieve complete conformal (coating thickness of 10–50 μm) encapsulation of model beads with the cross-linked PEG hydrogels.

Optimization of the Conformal Coating Process on Islets. The process for conformal coating was further optimized using multiple sources of islets of Langerhans, examining completeness of coating and the effect of the procedure on islet viability and function in vitro (GSIR).

In initial coating attempts with 10% (wt/vol) PEG-VS, phase-contrast and confocal images of islets coated with fluorescently labeled hydrogels demonstrated that the procedure was readily transferable to coating primary pancreatic islets (Fig. 2 *D–F*). Islet function in these examples, however, was determined to be compromised.

Step-by-step procedural testing was implemented to determine the effect of each variable of the encapsulation purification process on islet function, with GSIR and coating imaging as the experimental outcomes. The factor with the greatest negative impact on islet viability and function was the concentration of TEOA in the collection vessel. Decreasing the concentration from 0.1 to 0.02% (vol/vol) greatly improved islet function, as indicated by GSIR (Fig. 2*G*) for both human and rat islets ($P < 0.01$). We further confirmed that proper TEOA concentration was critical to islet viability and function by putting islets through the encapsulation and purification process in the absence of coating polymers and observing that 0.1% TEOA was detrimental (Fig. 2*G*).

To explore any potential detrimental impact of the residual oil (PPG) phase from the encapsulation process, final processing with or without hexane (which was used to extract PPG completely from the water phase) was carried out. As indicated by GSIR results, purification of encapsulated islets through hexane extraction of PPG did not have an impact on the in vitro function of the coated islets, whereas function was decreased when hexane was not used (Fig. 2 *H* and *I*; $P < 0.05$).

These adjustments (utilization of 0.02% TEOA in the oil phase in the collection vessel and final removal of the oil phase using a hexane wash) improved outcomes, as measured by functional assessment, and allowed for reproducible conformal coating of human, NHP, and rat islets when 10% (wt/vol) PEG-VS polymer and DTT cross-linker were used (Fig. 2*J*; $P > 0.05$).

Optimization of Hydrogel Composition for Conformal Coating of Islets. Following optimization of conditions for generating conformal coatings on islets, the next phase focused on selection of the appropriate biomaterials and cross-linking strategies to achieve stable polymeric capsules of appropriate permeability. Both the composition and degree of cross-linking of coating hydrogels were investigated and were related to changes in islet functional outcomes and resulting coating permeability.

By increasing the concentration of PEG-VS from 10% to 20% (Fig. 3*A*; trend but $P > 0.05$) or by increasing the thickness of coatings (by making macrocapsules instead of conformal coatings; Fig. 3*B*), there was a concomitant decrease in islet function, as shown by elevated insulin secretion during the second basal glucose step of the GSIR, a profile indicative of dysfunctional and/or dying beta cells. These results indicate a benefit of thinner, less dense coatings. Decreasing the degree of DTT-mediated cross-linking of 10% PEG-VS by "capping" a portion of the VS functional groups on the eight-arm PEG-VS before DTT exposure did not affect the function of coated islets (Fig. 3 *C* and *D*; $P > 0.05$), suggesting that the cross-link density attained with the 10 kDa of PEG-VS was appropriate. Increasing the molecular weight (Mw) and/or branching of the cross-linking agent via linear (1 M_r of Mw) or multiarm (four-arm, 10 M_r and 20 M_r of Mw) PEG multithiol cross-linkers resulted in no statistically significant change in islet GSIR function (Fig. 3*E*; $P > 0.05$). The addition of 0.8% or 0.4% ALG to 5% PEG-VS improved the function of the encapsulated islets compared with 5% PEG-VS alone, although this improvement was not observed for 10% PEG-VS-ALG (Fig. 3*F*; $P < 0.01$). Islet functional assessment results positively correlated with the permeability to 10 kDa of FITC-dextran, as a model permeant molecule, of the PEG coatings with different composition (Fig. 3*G*). The addition of ALG to the PEG-VS hydrogel precursor increased coating permeability. Based on these results, 5% PEG-VS with 0.8% wt/vol MVG

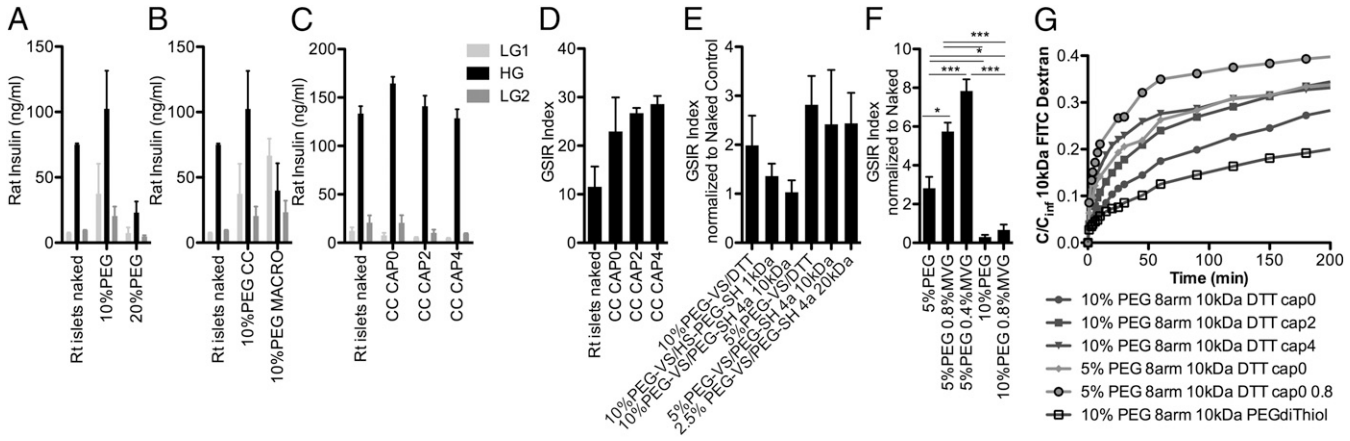

Fig. 3. Optimization of hydrogel composition for conformal coating of islets. (*A*) Effect of percentage of PEG-VS ($P > 0.05$). (*B*) Effect of coating thickness: conformal coating (CC) vs. macrocapsule (MACRO, diameter: 600–1,000 μm). (*C* and *D*) Effect of saturating (CAP) zero, two, or four of the eight functional groups of PEG-VS with CC. (*E*) Combined effect of cross-linker: DTT vs. 1-kDa linear PEG dithiol (HS-PEG-SH) vs. four-arm 10-kDa or 20-kDa PEG-SH and of PEG-VS percentage: 10% vs. 5%. (*F*) Effect of ALG (MVG) addition. Shown are mean ± SD with $n = 3$ for each value. (*G*) Diffusion of 10-kDa FITC-dextran outside of hydrogel microparticles with different PEG compositions as indicated by c/c_{inf} over time. c, concentration; c_{inf}, concentration of dextran at equilibrium. LG = 2.2 mM and HG = 16.7 mM. *$P < 0.05$; ***$P < 0.01$.

[medium viscosity ALG with 60% minimum glucuronate; Pronova] (PEG-ALG), cross-linked with a 4:1 molar ratio (3.1 mg/mL) of DTT, was selected as the optimal hydrogel configuration for further study.

Conformal Coating of Islets with PEG-ALG Does Not Impair in Vitro and in Vivo Function of Rodent Islets. Conformal coating with the optimized PEG-ALG formulation allowed for minimal coating thickness (typically a few tens of micrometers) encapsulation on rodent islets (Fig. 4*A*). No delay in insulin secretion during dynamic perifusion assessment was observed in the coated islets relative to uncoated controls (Fig. 4 *B* and *C*). Of interest, although uncoated islets gradually lost their GSIR function during extended in vitro culturing (Fig. 4*D*), this was not observed in PEG-ALG conformally coated islets (Fig. 4 *E* and *F*; $P < 0.05$). Timing of encapsulation after islet isolation was also a critical variable in postprocedural function: Islets encapsulated 48 h after isolation had improved GSIR function relative to those encapsulated after 24 h (Fig. 4 *G* and *H*; $P < 0.05$).

The very small thickness of the PEG-ALG conformally coated islets allowed correspondingly small transplant volumes to be placed in the renal subcapsular space to test function through transplantation of curative numbers of islets. To evaluate this, chemically induced diabetic mice were transplanted with either 700 or 1,500 syngeneic islet equivalents (IEQ) per mouse under the kidney capsule. Euglycemia (nonfasting blood glucose <200 mg/dL) was achieved and maintained for at least 112 d. Function was further confirmed by nephrectomy of the graft-bearing kidney and recipient reversion to hyperglycemia (Fig. 4*I*, arrows). Biocompatibility of PEG-ALG coatings analyzed with empty PEG-ALG capsules at day 7 and day 21 postimplantation and for PEG-ALG conformally coated syngeneic murine islet transplants at day 56 and day 116 posttransplantation was found to be strong, based on lack of fibrosis (Fig. S2*A*; H&E staining) and minimal detection of macrophages (Fig. S2*B*). Intact islets containing insulin$^+$ beta cells and glucagon$^+$ alpha cells were found in conformally coated grafts retrieved at day 56 and day 116, and were comparable to those observed in naked islet transplant controls (Fig. S2*C*). CD31$^+$ lymphatic vessel endothelial hyaluronan receptor 1 negative (Lyve-1) blood (Fig. S2*D*) and CD31$^+$Lyve-1$^+$ lymphatic (Fig. S2*E*) vessels were observed between the implanted capsules but not within them.

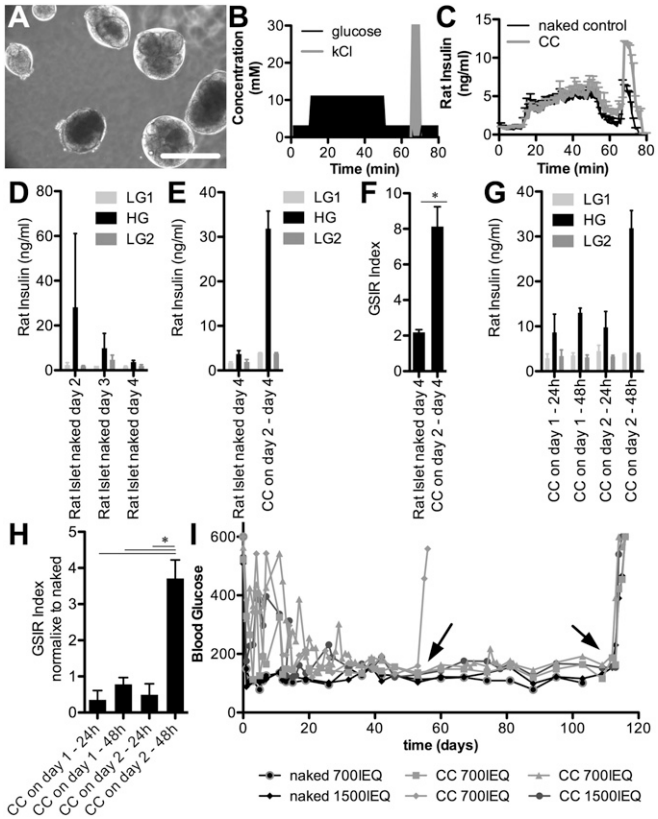

Fig. 4. Conformal coating of rodent islets with 5% (wt/vol) PEG-VS/DTT and 0.8% MVG (PEG-ALG) does not impair in vitro and in vivo function in mice. (*A*) Phase-contrast image of rat islets conformally coated (CC) with PEG-ALG. (Scale bar, 200 μm.) Perifusion schematic (*B*) and results (*C*) of PEG-ALG CC rat islets compared with naked controls. Effect of ex vivo culture of rat naked islets (*D*) or CC (on day 2 after isolation) islets (*E* and *F*) on GSIR up to day 4 after isolation. (*G* and *H*) Effect of timing on GSIR of rat CC islets either day 1 or day 2 after isolation and assessed either 24 h or 48 h after encapsulation. Shown are mean ± SD with $n = 3$ for each value. LG = 2.2 mM and HG = 16.7 mM. $*P < 0.05$; $***P < 0.01$. (*I*) Blood glucose of streptozotocin-induced diabetic C57BL/6 mice transplanted with either 700 or 1,500 IEQ of syngeneic naked control islets ($n = 2$) or PEG-ALG CC islets under the kidney capsule ($n = 4$). Nephrectomies were performed at day 52 and day 112 (arrows).

Discussion

A significant issue limiting the efficacy of correction of type 1 diabetes following the transplantation of encapsulated islets has been the relatively large size of the capsules generated via conventional microencapsulation. In traditional approaches, islets are incorporated within capsules of uniform size, determined by the geometry of a destabilized jet-forming apparatus. As such, the capsule size is adapted for the largest of islets, resulting in thick capsules on the majority of the islets. The thick capsules increase the volume of the total transplant, thus limiting selection of transplant sites; additionally, the thick layer of stagnant water created by the capsule increases transport limitations. To address this issue, we designed and implemented an encapsulation method that has the potential to overcome many of the limitations of prior methods. The presented flow-focusing approach creates a thin film of a water phase upon individual islets suspended within an oil continuous phase. Rather than the total diameter being determined by the encapsulation parameters, the thickness of a conformal coating is determined by the geometry, viscosity ratios, interfacial tension, and flow rate ratios of the process, with the overall diameter being determined by the individual islet diameter. This results in coatings with consistent thickness, independent of islet diameter. In the process we have developed, the conformal water phase contains a hydrogel precursor (PEG-ALG). In this approach, the precursor is converted to a gel upon a pH change initiated by exposure to a diffusible component within the oil phase. Using thiol-mediated (using DTT as a dithiol) cross-linking of a reactive multiarm PEG (using VS moieties), rapid gelation was achieved without cytotoxicity or loss of islet function.

One important challenge facing islet encapsulation therapies is the delayed insulin secretory response to glucose challenge (41, 42). Traditional microencapsulation methods are plagued by such delays, which are the combined result of limited polymer permeability and increased diffusional distances (43). In our hands, minimizing the coating thickness to a few tens of microns in thickness, and thereby the diffusional distance, despite the decreased permeability compared with ALG, resulted in no observable delays in islet insulin secretory response to glucose stimulation.

Due to the intrinsic lack of size-limiting factors of the conformal coating encapsulation technology that we have presented here, we were able to transplant conformally coated islets at curative doses in sites not accessible with standard microencapsulation methods, such as the renal subcapsular space. Lack of fibrosis and a necrotic core suggest that conformal coating with the PEG-ALG successfully addressed issues of both biocompatibility and diffusion limitations.

Materials and Methods

Inputs for the computational model in Comsol multiphysics were based on the model from Suryo and Basaran (38). Functionalization of eight-arm 10-kDa PEG (Jenkem Technology) with VS (Sigma) was achieved by Michael-type addition of VS. Gelation of PEG-VS was achieved by cross-linking with DTT (Sigma), 1-kDa PEG dithiol (HS-PEG-SH), or a 2:1 molar ratio of four-arm 10-kDa PEG thiol (PEG-SH) or four-arm 20-kDa PEG-SH (CreativePEGworks), adjusting the final pH to 7.4 through addition of TEOA (Sigma) to the collection bath (Fig. 2 *A*, e). Islet-sized polystyrene beads (PolySciences, Inc.) were suspended at 20–40% (wt/vol) and islets at 25,000–75,000 IEQ/mL in a solution of 2.5–20% (wt/vol) eight-arm 10-kDa PEG-VS and cross-linker with 0.4–0.8% (wt/vol) UP-MVG grade ALG (Pronova) in RPMI for selected experiments at pH 6, and were injected through a 16-gauge i.v. catheter (Fig. 2 *A*, c) at constant flow rate of 10 μL/min. An external oil phase of PPG with Mw = 3,500 with 10% (vol/vol) Span80 (Sigma) was flowing coaxially at the constant rate of 3.5 mL/min. Coated beads/islets were separated from the oil phase by hexane extraction. GSIR and perifusion were performed to assess the function of encapsulated islets. Islets were isolated from C57BL/6 mice as described elsewhere (44). Chemically diabetic C57BL/6 mice received 700–1,500 IEQ of C57BL/6 mouse islet grafts under the kidney capsule as described elsewhere (44). Data are presented as mean ± SD (Student *t* test or one-way ANOVA). Details of these procedures are provided in *SI Materials and Methods*.

ACKNOWLEDGMENTS. We thank Dr. C. O'Neil and Dr. K. G. Asfura for their help with PEG hydrogel chemistry; Dr. P. Buchwald for help with Comsol modeling; R. Lamazares and Dr. A. Zoso for help with the islet perifusion; the personnel of the Diabetes Research Institute (DRI) Preclinical Cell Processing and Translational Models Core for help with islet isolation, transplantation, and management/follow-up of diabetic mice; and the staff of the DRI Imaging Core. Funding was provided by the Diabetes Research Institute Foundation, the Juvenile Diabetes Research Foundation and the Leona M. and Harry B. Helmsley charitable trust (Grant 17-2010-5), Children with Diabetes, and Converge Biotech, Inc.

1. Gibly RF, et al. (2011) Advancing islet transplantation: From engraftment to the immune response. *Diabetologia* 54(10):2494–2505.
2. O'Sullivan ES, Vegas A, Anderson DG, Weir GC (2011) Islets transplanted in immunoisolation devices: A review of the progress and the challenges that remain. *Endocr Rev* 32(6):827–844.
3. Gray DW (1997) Encapsulated islet cells: The role of direct and indirect presentation and the relevance to xenotransplantation and autoimmune recurrence. *Br Med Bull* 53(4):777–788.
4. Basta G, Calafiore R (2011) Immunoisolation of pancreatic islet grafts with no recipient's immunosuppression: Actual and future perspectives. *Curr Diab Rep* 11(5): 384–391.
5. Duvivier-Kali VF, Omer A, Parent RJ, O'Neil JJ, Weir GC (2001) Complete protection of islets against allorejection and autoimmunity by a simple barium-alginate membrane. *Diabetes* 50(8):1698–1705.
6. Chang TM (1964) Semipermeable microcapsules. *Science* 146(3643):524–525.
7. Dufrane D, Goebbels RM, Gianello P (2010) Alginate macroencapsulation of pig islets allows correction of streptozotocin-induced diabetes in primates up to 6 months without immunosuppression. *Transplantation* 90(10):1054–1062.
8. Souza YE, et al. (2011) Islet transplantation in rodents. Do encapsulated islets really work? *Arq Gastroenterol* 48(2):146–152.
9. Suzuki K, Bonner-Weir S, Hollister-Lock J, Colton CK, Weir GC (1998) Number and volume of islets transplanted in immunobarrier devices. *Cell Transplant* 7(1):47–52.
10. Calafiore R, et al. (2006) Microencapsulated pancreatic islet allografts into non-immunosuppressed patients with type 1 diabetes: First two cases. *Diabetes Care* 29(1): 137–138.
11. Tuch BE, et al. (2009) Safety and viability of microencapsulated human islets transplanted into diabetic humans. *Diabetes Care* 32(10):1887–1889.
12. Elliott RB, et al. (2007) Live encapsulated porcine islets from a type 1 diabetic patient 9.5 yr after xenotransplantation. *Xenotransplantation* 14(2):157–161.
13. Colton CK (1995) Implantable biohybrid artificial organs. *Cell Transplant* 4(4):415–436.
14. Williams SJ, et al. (2010) Reduction of diffusion barriers in isolated rat islets improves survival, but not insulin secretion or transplantation outcome. *Organogenesis* 6(2): 115–124.
15. Buchwald P (2011) A local glucose-and oxygen concentration-based insulin secretion model for pancreatic islets. *Theor Biol Med Model* 8:20.
16. Colton CK, Avgoustiniatos ES (1991) Bioengineering in development of the hybrid artificial pancreas. *J Biomech Eng* 113(2):152–170.
17. Calafiore R (1997) Perspectives in pancreatic and islet cell transplantation for the therapy of IDDM. *Diabetes Care* 20(5):889–896.
18. Elliott RB, et al. (2005) Intraperitoneal alginate-encapsulated neonatal porcine islets in a placebo-controlled study with 16 diabetic cynomolgus primates. *Transplant Proc* 37(8):3505–3508.
19. Mørch YA, Donati I, Strand BL, Skjåk-Braek G (2006) Effect of Ca2+, Ba2+, and Sr2+ on alginate microbeads. *Biomacromolecules* 7(5):1471–1480.
20. Teramura Y, Iwata H (2010) Bioartificial pancreas microencapsulation and conformal coating of islet of Langerhans. *Adv Drug Deliv Rev* 62(7-8):827–840.
21. Chabert M, Viovy JL (2008) Microfluidic high-throughput encapsulation and hydrodynamic self-sorting of single cells. *Proc Natl Acad Sci USA* 105(9):3191–3196.
22. Lee DY, Park SJ, Nam JH, Byun Y (2006) A new strategy toward improving immunoprotection in cell therapy for diabetes mellitus: Long-functioning PEGylated islets in vivo. *Tissue Eng* 12(3):615–623.
23. Krol S, et al. (2006) Multilayer nanoencapsulation. New approach for immune protection of human pancreatic islets. *Nano Lett* 6(9):1933–1939.
24. Wilson JT, Cui W, Chaikof EL (2008) Layer-by-layer assembly of a conformal nanothin PEG coating for intraportal islet transplantation. *Nano Lett* 8(7):1940–1948.
25. Kizilel S, et al. (2010) Encapsulation of pancreatic islets within nano-thin functional polyethylene glycol coatings for enhanced insulin secretion. *Tissue Eng Part A* 16(7): 2217–2228.
26. Teramura Y, Kaneda Y, Iwata H (2007) Islet-encapsulation in ultra-thin layer-by-layer membranes of poly(vinyl alcohol) anchored to poly(ethylene glycol)-lipids in the cell membrane. *Biomaterials* 28(32):4818–4825.
27. Gattás-Asfura KM, Stabler CL (2013) Bioorthogonal layer-by-layer encapsulation of pancreatic islets via hyperbranched polymers. *ACS Appl Mater Interfaces* 5(20): 9964–9974.
28. Cruise GM, Scharp DS, Hubbell JA (1998) Characterization of permeability and network structure of interfacially photopolymerized poly(ethylene glycol) diacrylate hydrogels. *Biomaterials* 19(14):1287–1294.
29. Hill RS, et al. (1997) Immunoisolation of adult porcine islets for the treatment of diabetes mellitus. The use of photopolymerizable polyethylene glycol in the conformal coating of mass-isolated porcine islets. *Ann N Y Acad Sci* 831:332–343.
30. Leung A, et al. (2005) Emulsion strategies in the microencapsulation of cells: Pathways to thin coherent membranes. *Biotechnol Bioeng* 92(1):45–53.
31. Cruise GM, Hegre OD, Scharp DS, Hubbell JA (1998) A sensitivity study of the key parameters in the interfacial photopolymerization of poly(ethylene glycol) diacrylate upon porcine islets. *Biotechnol Bioeng* 57(6):655–665.
32. Wyman JL, Kizilel S, Skarbek R, Zhao X, Connors M, et al. (2007) Immunoisolating pancreatic islets by encapsulation with selective withdrawal. *Small* 3(4):683–690.
33. Lee DY, Park SJ, Lee S, Nam JH, Byun Y (2007) Highly poly(ethylene) glycolylated islets improve long-term islet allograft survival without immunosuppressive medication. *Tissue Eng* 13(8):2133–2141.
34. Hume PS, Bowman CN, Anseth KS (2011) Functionalized PEG hydrogels through reactive dip-coating for the formation of immunoactive barriers. *Biomaterials* 32(26): 6204–6212.
35. Dolgin E (2014) Encapsulate this. *Nat Med* 20(1):9–11.
36. Rabanel JM, Banquy X, Zouaoui H, Mokhtar M, Hildgen P (2009) Progress technology in microencapsulation methods for cell therapy. *Biotechnol Prog* 25(4):946–963.
37. Lin SP, Reitz RD (1998) Drop and spray formation from a liquid jet. *Annu Rev Fluid Mech* 30(1):85–105.
38. Suryo R, Basaran OA (2006) Tip streaming from a liquid drop forming from a tube in a co-flowing outer fluid. *Phys Fluids* 18(8):082102-13.
39. Anna SL, Bontoux N, Stone HA (2003) Formation of dispersions using "flow focusing" in microchannels. *Appl Phys Lett* 82(3):364–366.
40. Barrero A, Loscertales IG (2007) Micro- and nanoparticles via capillary flows. *Annu Rev Fluid Mech* 39:89–106.
41. Omer A, et al. (2004) Exercise induces hypoglycemia in rats with islet transplantation. *Diabetes* 53(2):360–365.
42. De Vos P, et al. (1996) Kinetics of intraperitoneally infused insulin in rats. Functional implications for the bioartificial pancreas. *Diabetes* 45(8):1102–1107.
43. de Vos P, Vegter D, Strubbe JH, de Haan BJ, van Schilfgaarde R (1997) Impaired glucose tolerance in recipients of an intraperitoneally implanted microencapsulated islet allograft is caused by the slow diffusion of insulin through the peritoneal membrane. *Transplant Proc* 29(1-2):756–757.
44. Pileggi A, et al. (2005) Prolonged allogeneic islet graft survival by protoporphyrins. *Cell Transplant* 14(2-3):85–96.